Desalination and Water Treatment
www.deswater.com

doi: 10.5004/dwt.2023.29993

312 (2023) 28–38
November

Green synthesis of iron-ore flat sheet membrane and physicochemical characterization

R. Chihi[a], P. Ugarte[b], M. Menendez[b], L. Mansour[c], F. Ayari[a,*]

[a]*Faculty of Sciences of Bizerte, LR 05/ES09 Laboratory of Applications of Chemistry to Resources and Natural Substances and to the Environment (LACReSNE), Carthage University, Zarzouna 7021, Tunisia, email: fadhilaayari@yahoo.fr (F. Ayari) ORCID ID: 0000-0002-3836-2029*
[b]*Aragón Institute of Engineering Research I3A, University of Zaragoza, 50018 Zaragoza, Spain*
[c]*Department of Zoology, College of Science, King Saud University, P.O. Box: 2455, Riyadh 11451, Saudi Arabia*

Received 22 April 2023; Accepted 19 September 2023

ABSTRACT

While ceramic membranes offer superior chemical and mechanical characteristics compared to their polymeric counterparts, their commercial availability comes with a significantly higher price tag. The exploration of cost-effective ceramic membrane alternatives, using affordable raw materials and production techniques that required lower manufacturing temperatures than conventional industrial ceramic membranes, holds the potential to deliver viable solutions for various applications. Iron ore is proposed in this work as raw material for the manufacture of low-cost ceramic membranes, because it is inherent structural and chemical properties and their low cost. Iron ore, as the starting material, was characterized using several techniques, including X-ray diffraction, X-ray fluorescence, Fourier-transform infrared spectroscopy, differential thermal analysis, and gas adsorption. Flat sheet membranes were successfully synthesized and characterized by mercury intrusion porosimetry, permporometry method, air and water permeation and scanning electron microscopy. The results confirm that a suitable pore size for the use of these ceramic membranes in microfiltration applications has been achieved. This development represents an energy economy in the manufacture of ceramic membranes and lower production cost by using cheap raw material, compared with the current technology.

Keywords: Ceramic membranes; Low-cost material; Iron ore; Bubble point method; Air and water permeation; Microfiltration

1. Introduction

Since their discovery in Tunisia in 1869 iron ore has attracted considerable attention. Tunisian iron production is around 9 million tons, as evaluated by the National Office of Mines (ONM). Owing to the high content of useful silica (SiO_2), alumina (Al_2O_3), magnetite (Fe_3O_2), hematite (Fe_2O_3) and clay in the natural starting material, makes perfect economic outlook to recover those minerals for new industrial applications, not only for iron production.

In recent decades, ceramic membranes have experienced significant transformation, expanding beyond their initial niche applications, including the nuclear industry, to find diverse uses in fields such as chemistry, food industries, as well as industrial, agricultural, and domestic wastewater treatment [1].

Ceramic membranes offer enhanced chemical and mechanical properties in comparison to polymeric membranes. However, their utilization is constrained by their notably higher cost, typically exceeding that of polymeric membranes by an order of magnitude. This cost

* Corresponding author.

disparity arises from the utilization of expensive materials like high-purity alumina, titania, or zirconia, as well as their processing through sintering at extremely high temperatures. To address this issue, there has been a shift towards the development of cost-effective ceramic membranes, involving the use of more economical raw materials (e.g., clay) and organic pore-forming compounds (e.g., starch) (Table 1).

Samples were sintered from 850°C to 1,150°C for 2 h. The optimal membrane sintered at 1,050°C has a porosity of 34.5%, an average pore diameter of 3.9 μm, water permeability of 43.50 L/h/m^2·bar and mechanical strength of 26.7 MPa.

Our innovative concept revolves around the creation of a microfiltration ceramic membrane with high thermal stability, chemical inertness, good antimicrobial ability and high separation efficiency, by using iron ore as raw inexpensive and abundant material. The iron-ore mines not only can be comprehensively utilized, but also create maximum benefit by using natural starting material as membrane. Moreover, it has been chosen for its higher porosity, mechanical stability, low sintering temperature compared with pure oxides of titanium, zirconia, alumina and silica, and good chemical resistance.

The purpose of this present investigation is to develop low-cost ceramic membranes from iron ore materials. In particular, this work will examine the effect of varying the particle size of the starting material and the final heat treatment on the characteristics of pores size distribution, textural properties and morphology of the flat membrane made from such material.

We conducted a comprehensive analysis of the iron ore material through a range of techniques, including X-ray diffraction, X-ray fluorescence, Fourier-transform infrared spectroscopy, differential thermal analysis, and nitrogen adsorption at 77 K. Subsequently, the membranes we produced were subjected to characterization using mercury intrusion porosimetry, the gas–liquid displacement method, measurement of air and water permeation rates, and scanning electron microscopy to examine the inner surface.

2. Experimental set-up

2.1. Starting material

2.1.1. Raw material

The raw natural material used to prepare ceramic membranes was collected from iron-ore quarry situated at Tamra region in the north–west of Tunisia. The starting material was dried after collection and crushed into small fragments, grounded into powder and sieved in the range of (60–250 μm). Two different sizes of particles have been used, labeled Iron$_{BS}$ for particles in the range of (60–250 μm) and Iron$_{SS}$ for particles smaller than 60 μm.

The sample X-ray diffraction was obtained with a commercial instrument (ARL 9900 of Thermo Fisher, United States) with monochromatic radiation K_{al} of cobalt (λ = 1.78 Å). The major chemical composition of iron ore was determined by X-ray fluorescence analysis (ARL 9900, Thermo Fisher Scientific, United States) with monochromatic radiation K_{al} of cobalt (λ = 1.78 Å). The result of the investigation has been given in weight as follows: Fe_2O_3 (64.12 wt.%), SiO_2 (13.66 wt.%), CaO (6.29 wt.%). It contains also Al_2O_3 (3.90 wt.%), Na_2O (3.90 wt.%), MnO (1.44 wt.%) and low quantities of MgO (0.69 wt.%), TiO_2 (0.23 wt.%) and P_2O_5 (0.15 wt.%) with an ignition loss equal to 9.01%.

2.1.2. Mineralogical composition

Mineralogical analysis of starting powder materials at 298 K was carried out using PANalytical X'Pert HighScore plus diffractometer with CuKα radiation (λ = 1.5406 Å). The peaks in X-ray diffraction (Fig. 1), reveal the presence of the following phases: goethite FeOOH (2θ = 21.2°, 34.96°, 36.8°, 41.4°, 50.5°, 53.2° and 59.3°) and hematite Fe_2O_3 (2θ = 33.22°, 40.5° and 68.3° [16–18]. Furthermore, a small quantity of kaolinite is distinctly noticeable alongside quartz, which appears as a minor phase.

2.1.3. Fourier-transform infrared spectroscopy analysis

Infrared spectra of iron-ore material was collected on a PerkinElmer 783 over 400–4,000 cm^{-1} spectral range (Fig. 2). The samples were prepared as KBr pellets. Generally, goethite can be differentiated from other compounds by an intense broad band due to the bulk hydroxyl stretch at 3,170 cm^{-1} [19] and two far less intense bands at 3,660 and 3,484 cm^{-1} that can be attributed to the surface hydroxyl groups [20]. Goethite can also be identified by its two standards OH bending bands at *ca.* 910 cm^{-1} (γ-OH) and 816 cm^{-1} (δ-OH) [20,21].

The most characteristic infrared adsorption bands of hematite are present in the low frequency region (<600 cm^{-1}). Infrared vibrations of hematite formed from the Si-free hydrite are illustrated with two intense bands at 478, 574 and 620 cm^{-1} [22,23].

Kaolin is similarly present and identified by the presence of peaks at 1,032 cm^{-1} (Si–O–Si), 1,011 cm^{-1} (Si–O–Al) and 940 cm^{-1} (Al–O–H). The presence of C=O species is revealed by the existence of band at 1,451 cm^{-1}, which corresponds to asymmetric stretching vibration.

2.1.4. Brunauer–Emmett–Teller specific surface area and pore size distribution

Adsorption of gases and vapors is one of the most widely used techniques for the characterization of porous material. The Brunauer–Emmett–Teller (BET) gas adsorption theory is the foundation for the measurement of surface area in high specific surface materials. The textural parameters of iron ore material were obtained from the adsorption and desorption isotherms of N_2 at 77 K using a Quantachrome Model Nova 1200e Surface (Germany) and porosity analyser. The BET adsorption–desorption isotherms exhibited by our sample (Fig. 3) are classified as type IV, in accordance with International Union of Pure and Applied Chemistry guidelines [24], indicating the mesoporous nature of this sample. The main textural properties obtained from this technique are summarized in Table 2. The pore size distribution curve, as derived from the nitrogen sorption data (Fig. 4), illustrates a narrow pore size distribution with a diameter of 19 Å (as indicated in Table 2). Hence, this sample is highly suitable as a natural porous material for membrane preparation.

Table 1
Summary of membrane characteristics using different process and starting materials

References	Materials used	Configuration of the membrane	Firing temperature	APS (μm)	Water permeability	Air permeability	Mechanical properties/ Thickness	Applications
Palacio et al. [2]	Moroccan ores, clay And micronized phosphate Starch as organic additives	Flat disk filters	1,250°C		16 ms/Pa × 10^{-8}	1.6 L/min/ cm^2·bar		Wastewater treatments for Moroccan textile industry
Bouzerara et al. [3]	Kaolin and kaolin-doloma mixtures Natural abundance (low price) and their beneficial properties	Tubular (extension method) and flat (dry-pressing)	1,250	Process 2, 22.31 (PV%, 22.31) Process 3, 27.72 (PV%, 43)			16 MPa	Supports of membranes of microfiltration and ultrafiltration
Masmoudi et al. [4]	Support, cordierite Active layer, synthesized lacunary hydroxyapatite (HA)	Support, tubular	600	Support, 7 Layer, 0.5 (PV%, 48)			32.5 μm	Treat cuttlefish effluents generated from the conditioning seawater products
Harabi et al. [5]	Support, raw kaolin and lime extracted from limestone Active membrane, CaO, Al_2O_3·$2SiO_2$	Tubular membrane support	Support, 1,000°C Layer, 850°C	Support, 7 μm, (PV% 48) Membrane, 0.5 μm (PV% 50)			30 MPa Microfiltration layer, 33 μm	
Majouli et al. [6]	Support, Moroccan perlite organic additives	Flat	Support, 1,000°C	Support, 6.64 μm (PV%, 41.8)	Support, 1,797 L/h/m^2·bar	–	–	Applied for treatment of wastewater
Boulkrinat et al. [7]	Support, natural aluminosilicate with quartz and calcite Intermediate layer, titania Top layer, halloysite	Nanotubes (halloysite), extrusion method	Support, 1,350°C–1,425°C Intermediate layer, 1,050°C Top layer, 580°C	Support, 6–13 μm (PV%, 48–46) Intermediate layer, 0.8 μm Aluminosilicate top layer	Support, 22,000 L/h/m^2·bar and 210 L/h/m^2·bar	–	14–17 MPa Titania layer, 40 μm Aluminosilicate top layer, 20 μm	Separation of macromolecular proteins
Majouli et al. [8]	Support, Moroccan perlite Organic additives: methocel, amijel, starch and PEG	Flat	1,000°C	6.64 μm, (PV%, 41.8)	1,797 L/h/m^2·bar	–	–	Used to clarify a suspension of backing powder
Bouzerara et al. [9]	Clay and calcium carbonate mixtures Organic additives: amijel, methocel and starch Layer, zirconia	Tubular configuration Layer, slip casting process	Support, 1,250°C Layer, 1,050°C	Support, 3.4 μm, (PV%, 52) Layer, 0.16 μm	1,000 L/h/m^2·bar	–	Membrane, 25 μm	Effluent treatment

Table 1 (Continued)

Table 1

References	Materials used	Configuration of the membrane	Firing temperature	APS (μm)	Water permeability	Air permeability	Mechanical properties/ Thickness	Applications
Harabi et al. [10]	Support, kaolin and calcium carbonate mixtures	Tubular configuration, extrusion method	1,150°C–1,250°C	3.91–8.56 μm, (PV%, 42–50.4) 1.3	–	–	67–77 MPa	Applied for micro or ultrafiltration
Boudaira et al. [11]	Support, kaolin and calcite mixtures Layer, zirconium oxide	Support, tubular configuration Layer, slip casting technique	Support, 1,250°C Layer, 1,150°C	Support, 4 μm (PV%, 52) Layer, 0.35 μm	Membrane, 1,440 L/h/m^2·bar	–	23 MPa Layer, 24 μm	Applied for ultrafiltration
Bouazizi et al. [12]	Support, bentonite with micronized phosphate (30 wt.%) thin layer with TiO_2	Support, disk Layer, spin-coating technique	Support, 950°C Layer, 800°C	Support, 1.8 μm (PV%, 34.06) Layer, 72 nm	Support, 725 L/h/m^2·bar Layer, 33 L/h/m^2·bar	–	14.6 MPa	Applied for dye removal
Saja et al. [13]	Natural perlite (5 wt.%) starch as porosity agent	Flat membrane	950°C	1.7 μm, (PV%, 52.11)	1,433.46 L/h/m^2·bar	–	21.68 MPa 2.2 ± 0.3 mm	Industry wastewater effluents (agro-food and tannery effluents)
Fang et al. [14]	Support, fly ash with methyl-cellulose and water Layers of fly ash (cc, 10 wt.%) Top layer, fly ash with Lomar-D and DSX 3290	Tubular configuration Layers, slip casting process	Support, 1,190°C Layer, 1,150°C Top layer, 1,000°C	Support, 2.13 μm Layer, 1.94 μm Top layer, 0.77 μm	Support, 2.26 × 10^4 L/h/m^2·bar Layer, 1.86 × 10^4 L/h/m^2·bar Top layer, 1.56 × 10^4 L/h/m^2·bar	–	Support, 2.13 μm Layer, 30 μm Top layer, 17 μm	Applied for textile industry
Chihi et al. [15]	Support, bentonite clay Organic additives, amijel, methocel, starch	Tubular configuration	1,000°C	1.7 μm	525 L/h/m^2·bar	–	24 MPa	Applied to textile industry
Lagdali et al. [36]	Phengite clay	Flat membrane	1,150°C	3.9 μm	43.50 L/h/m^2·bar	–	26.7 MPa	Pre-treated real wastewater

APS – Average pore size, μm;
PV – Pore volume, %.

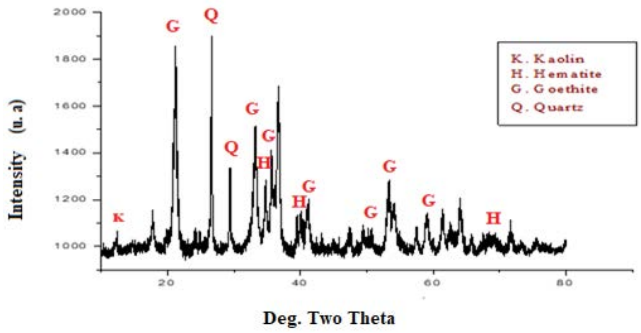

Fig. 1. X-ray diffraction pattern of iron ore.

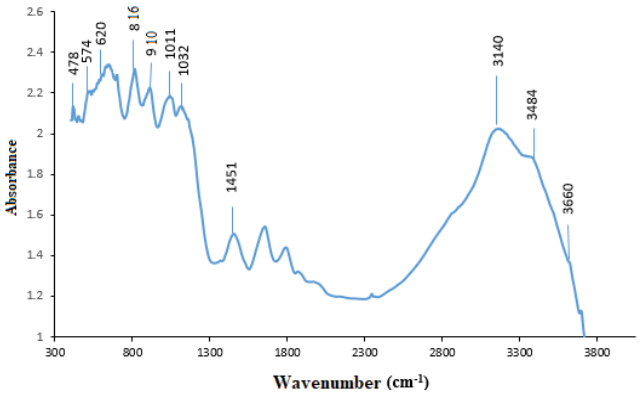

Fig. 2. Infrared spectra of iron ore.

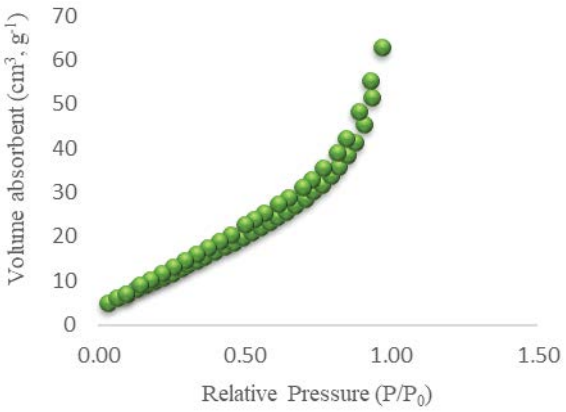

Fig. 3. Nitrogen adsorption–desorption isotherms at 77 K for iron-ore.

Table 2
Textural properties of iron-ore

	S_{BET} (m^2/g)	$S_{BJH/mesop}$ (m^2/g)	$V_{BJH/mesop}$ (cm^3/g)	V_{ads} (cm^3/g)	D (Å)
Iron ore sample	45.9	44.2	0.09	0.10	19

S_{BET} (m^2/g): BET surface area, $S_{BJH/mesop}$: mesopore surface area, $V_{BJH/mesop}$: mesopore volume, V_{ads}: volume of N_2 adsorbed at $P/P_0 = 0.98$, D: average pore diameter.

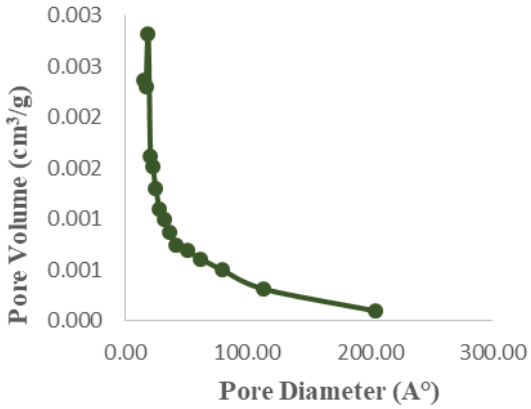

Fig. 4. Pore size distribution curve from nitrogen sorption data of iron-ore.

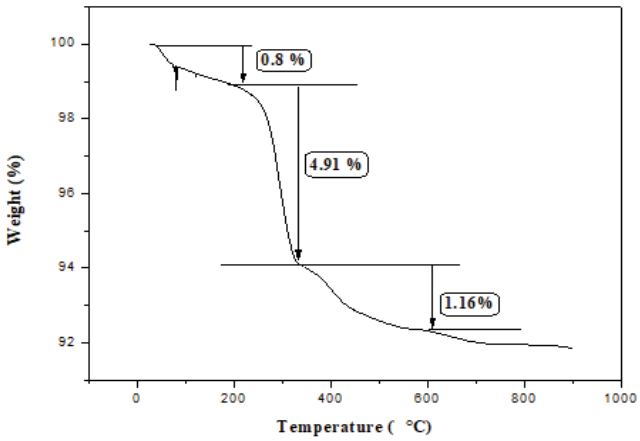

Fig. 5. Thermogravimetric analysis of iron ore material.

2.1.5. Thermogravimetric analysis

In the present investigation, iron ore thermal stability was studied in the temperature range of 298–1,173 K with heating rates of 5°C·min^{-1} using thermogravimetric analyses (Thermobalance L81, Linseis, Germany).

The thermogravimetric analysis of iron ore show three mass loss steps. The first one is between ambient to 423 K (Fig. 5). This mass loss (0.8%) is attributed to the loss of structural water after a dehydration reaction. The second step (4.91%) occurs from 473.15 to 623 K and is due to the mineralogical transformation of goethite into hematite [25]. The third mass loss step (1.16%) is attributed to the loss of molecular of oxygen corresponding to deshydroxylation, that profoundly changes the structure and leads to metastable states evolving towards a stable state [26,27].

2.2. Preparation of ceramic sheet membrane

The paste was synthesized from a mixture of natural iron ore and organic additives in an optimal formulation detailed in our previous work [15]. The binder, methocel, used in this study was trademarks of Dow Chemical Company, (France). Amijel (Cplus 12076) was employed

as a plasticizer, purchased from the Cerestar Company (France). Starch (RG 03408, Cerestar) was utilized as a porosity agent. Those organic additives are required to prepare a paste with suitable rheological properties. The mixture was homogenized with the addition of water in a stepwise manner. A block appeared at the end of this phase. For the preparation of plastic paste, an aging of 3 d under high humidity conditions is required to avoid premature drying and ensure the complete diffusion of water and organic additives. Then, the paste was shaped into cylindrical granules and later flattened using abrasive SiC discs. Flat sheet membranes were placed on stems at room temperature for 2 d to ensure a homogenous drying and avoid twisting and bending. Finally, membranes were sintered on electric oven with the adequate temperature program.

Thermal cycling was achieved in two steps: (a) annealing at 523 K for 2 h with a speed of 2°C/min to allow thermal decomposition of organic additives and (b) calcination at the desired temperature for 3 h at 5°C/min to avoid the formation of cracks in the samples.

2.3. Characterization of flat sheet membrane

2.3.1. Mercury intrusion porosimetry

Mercury intrusion porosimetry has been routinely employed to evaluate the pore size distribution of powdered and bulk materials with open and interconnected pore structures. This technique was proposed by Liabastre and Orr [28], then developed by Lowell and Shields [29] and applied for the first time to characterize membrane filters by Honold and Skau [30]. Mercury intrusion measurements were obtained with an AutoPoreIV9500 (Micromeritics Inc., USA).

2.3.2. Bubble point method and extended bubble point method

Bubble point method allows to determination of membrane air permeance and also provides information about the pores that are controlling the permeance. Bubble point method measures the minimum pressure necessary to blow the firstly observed air bubble that correspond to the largest pore size of the membrane, this value is known as bubble point. This method is used to measure pores with size above 50 nm and is standardized by ISO 2942 and ISO 4003 and is probably the most employed technique to measure defects in microfiltration membranes.

Mathematical relationship between pressure and pore size is given by Washburn equation:

$$\Delta P = \frac{4\gamma\cos\theta}{d_p}$$

where ΔP is the transmembrane pressure, γ is the surface tension in the gas–liquid interface, θ is the contact angle and d_p is the pore diameter. For wetting liquids, θ is taken as 0 [31,32].

Average pore size (d_{50}) is calculated with Washburn's equation from the pressure at the intersection point of the line that corresponds 50% of air flow (mL/min) through the dry membrane vs. the applied pressure when the membrane is wet (Fig. 6). In a similar way, d_{15} d_{25} and d_{75} have been calculated.

The experimental set up consists of gas pressure vessel, pressure regulator and indicator, membrane holder and a flow meter (Fig. 7). The model system, including housing and seal was tested several times to avoid the existence of any leaks. Water or isopropanol were employed as wetting liquids. The low interfacial tension between isopropanol and air allows us to perform measurements of very small pores with no needs of high pressures, which can be an important consideration regarding the mechanical integrity of the membrane.

According to the process of manufacture two series of membranes were investigated using different particle size (60 and 250 μm), labeled $Iron_{SS}$ and $Iron_{BS}$, respectively.

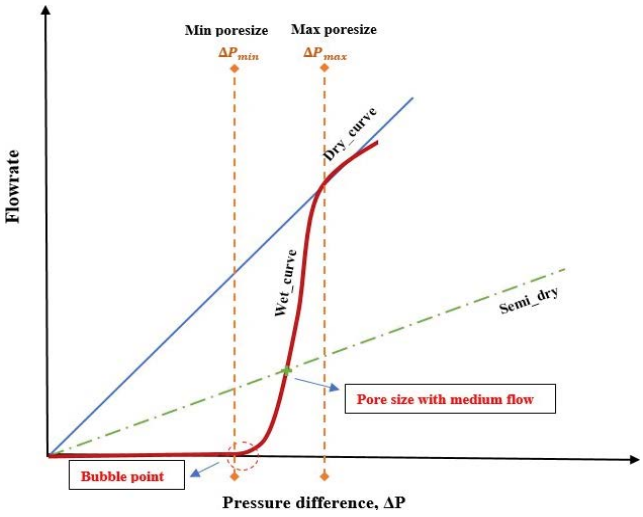

Fig. 6. Theoretical flow-pressure curve from the measurement of gas permeation.

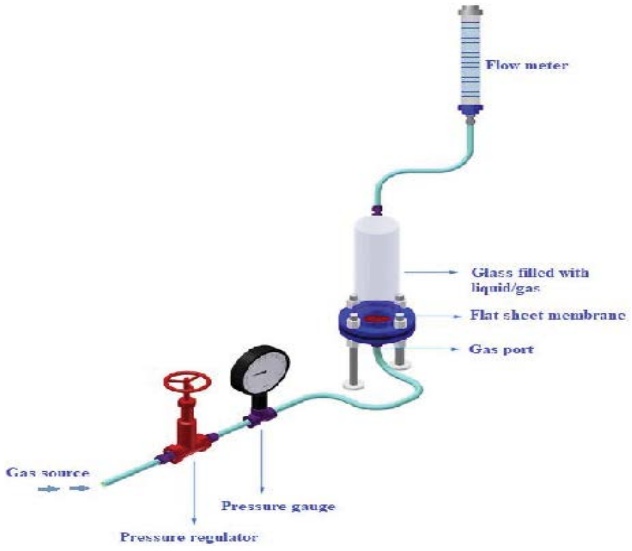

Fig. 7. Scheme of bubble gas transport test equipment for flat sheet membrane.

3. Results and discussions

3.1. Mercury intrusion measurements

Pore size distribution analysis was conducted for both $Iron_{SS}$ and $Iron_{BS}$. Figs. 8 and 9, along with Table 4, present the results of mercury porosimetry, highlighting the mean pore diameter for membranes crafted from smaller particle sizes. As one might anticipate, elevating the sintering temperature generally leads to an increase in the average pore size and a reduction in total porosity, indicative of agglomeration phenomena (as detailed in Table 4 and illustrated in Fig. 8).

Conversely, Fig. 9 demonstrates that the pore size distribution remains relatively uniform, encompassing a diverse range of pore sizes. This phenomenon is likely attributed to the presence of larger particles ($Iron_{BS}$). The decline in porosity suggests that particles tend to approach one another at higher sintering temperatures.

3.2. Bubble point method and extended bubble point method

In order to test pore size and pore size's distribution of our synthesized membranes, we have been compared the flow rate vs. pressure profile of a dry membrane with that of a wetted membrane by gas–liquid displacement porosimetry.

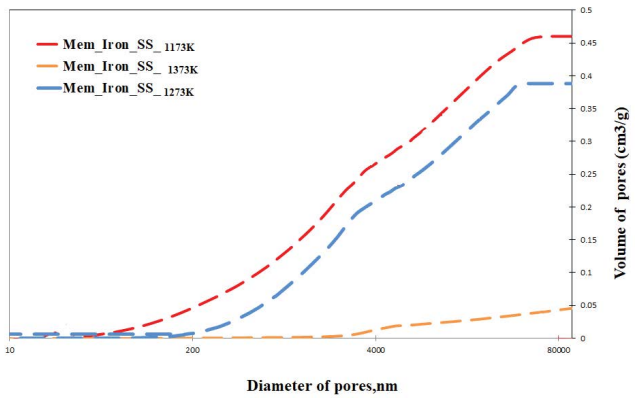

Fig. 8. Pore size distribution at different calcination temperature (1,373; 1,273 and 1,173) with small particle size by mercury porosimetry method.

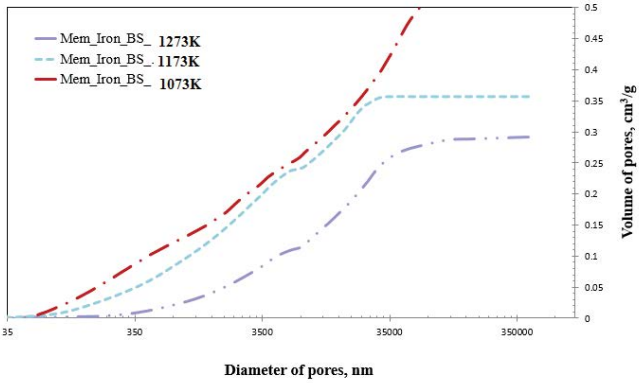

Fig. 9. Pore size distribution at different calcination temperature (1,273; 1,173 and 1,073 K) with big particle size by mercury porosimetry method.

The Laplace equation suggests that the method is independent of the liquid type used. However, if different liquids are used, different radiuses will be obtained for the pore radius, which is probably due to wetting effects of the liquid to membrane material [33]. The wetting effect of a liquid can be estimated by surface tension values. The value of surface tension can affect the pressure needed to achieve and measure the lowest pores sizes. Since the pressure value needed for liquid displacement is proportional to the surface tension, the selection of liquid will limit the minimum pore size could be characterized. For such a system, the fluids used to measure sample fired at 1,273 K using big size particles present two different interfacial tension, isopropanol (23.0 mN/m) and water (72.8 mN/m) [34]. With higher water interfacial tension, the system needs high pressure for gas permeation through small pores. The medium pore size reached was 9.09 micron. Using isopropanol, as fluid with lowest interfacial tension, can achieve smaller ones and reach 5.43 micron as medium pore's size.

According to the pore-forming mechanism and membrane sintering, the particle size of the raw material affect to the pore size distribution of the membrane. Table 5 shows the results of pore size distribution of the membranes. For both kind of membranes, an increase of temperature promote the increase of the pore size. High temperature would melt some crystals generating small pores that combining with each other will form large pores. Except for $Iron_{BS}$ sintered at 1,073 K that pore size increase, suggesting defects in the sintering process that translate into high pore size.

Table 3
Different conditions for several tests

Type of samples	Firing temperature (K)	Wetting solution used
	1,373	Isopropanol[a]
$Iron_{SS}$	1,273	Isopropanol
	1,173	Isopropanol
$Iron_{BS}$	1,273	Isopropanol and water[b]
	1,173	Isopropanol
	1,073	Isopropanol

[a]Surface tension of isopropanol is 21.7 dyn/cm at 293 K.
[b]Surface tension of water is 73 dyn/cm at 293 K.

Table 4
Diameter pores measured by mercury porosimetry of iron's membranes using two kind of manufacturing process

	Firing temperature (K)	Diameter of pores (μm)
$Iron_{SS}$	1,373	(3.4–3.9)
	1,273	(1.6–1.8)
	1,173	(2.0–2.3)
$Iron_{BS}$	1,273	(3.6–4.5)
	1,173	(3.1–4.1)
	1,073	(2.1–4.2)

Also, we can observe that for membranes with large particle size ($Iron_{BS}$) the pore size was higher than for membranes with small particles ($Iron_{SS}$). With the decrease of the particle size of the raw material, pore size formed by accumulation becomes smaller so the pore size of the membrane gradually decreases. The pore size ranges from 0.76 to 5.43 μm for $Iron_{SS}$ and $Iron_{BS}$ sintered both at 1,373 K. Also, the membranes with particle size show a narrow pore size distribution compared with membranes with particle size.

The data obtained with $Iron_{BS}$ correspond with mean size pores acquired with mercury porosimetry. The slight deviations are in the range of the experimental error. Unfortunately, our experimental set up for some samples was limited for high pressure and the flow-pressure curve does not reached its dry flow behavior up to this pressure.

The membranes fired at 1,273 K with smaller particle size were tested with air-water displacement porosimetry and mercury porosimetry in order to compare both methods; these results are as well presented in Table 5. The previous experiments have shown that the mean pore size ranges from 0.76 μm to approximately 3.6 μm, by air-water displacement porometry and mercury porosimetry analysis, respectively.

Based on data obtained, the results of porometry and mercury porosimetry are not in good agreement with each other. The difference has been interpreted and explained in the study of Rahman et al. [35] by the way that the use of bubble point method explain more the morphology of the different pores present in the model studied point which controlling the permeation. In addition, if we have large and small pores in series, mercury porosimetry will detect both, but air-water displacement technique will measure only the small pore, which is the one controlling the permeation.

Comparing the results obtained with those from literatures, a good agreement has been achieved with the results from other authors using different starting materials such as perlite [8] with mean pore size at around 6.64 μm, clay [9] with a support to approximately 3.4 μm and a using of zirconia layer with pores at around 0.16 μm, with kaolin [11] a support was made with mean pore size at around 4 μm and a zirconia layer of approximately 0.35 μm.

Table 5
Characteristics of membranes made from iron ores with different particle size

	$Iron_{SS}$			$Iron_{BS}$		
Diameter, cm	1.3			1.3		
Thickness, cm	0.2			0.3		
Temperature, K	1,373	1,273	1,173	1,273	1,173	1,073
$d_{p\ 15\%}$	1.5	1.1	0.6	24.8	7.2	26.3
$d_{p\ 25\%}$	1.4	0.9	0.4	21.7	6.7	25.5
$d_{p\ 50\%}$	–	0.8	–	5.4	5.8	24.8
$d_{p\ 75\%}$	–	–	–	1.7	3.1	19.2
Mercury porosimetry, μm	6.1	3.6	2.5	5.8	4.8	3.6
Air permeance, $\times 10^3$ L/h/m²·bar	2	–	–	$2*10^3$	856	850
Water permeance, L/h/m²·bar	281	–	–	222	149	–

3.3. Permeance: air and water measurements

The tests have been realized for all the membranes (Table 5). Results proved that the increase of applied pressure causes a linear increase of air flux. Higher values of air permeance were obtained with $Iron_{BS}$. These data show clearly the presence of big voids and pores that make membranes more permeable. The further sintering process causes an enlargement of diameter of pores and porosity.

For the membrane sintered at 1,273 K with $Iron_{SS}$, water permeance was found to be 280.68 L/h/m²·bar. Relatively higher permeance values were obtained from $Iron_{BS}$ at 1,273 and 1,173 K, being 222.57 and 149.36 L/h/m²·bar, respectively. As the sintering temperature decreases, the permeance increases.

The tests to determine permeance of $Iron_{BS}$ sintered at 1,073 K and $Iron_{SS}$ sintered at different temperature (Table 5), cannot provide any information because their fragile texture and/or the excessive agglomeration of particles at high temperature.

3.4. Scanning electron microscopy

Fig. 10 illustrates scanning electron microscopy images for the membranes sintered at different temperatures. For all membranes a surface with rough morphological structure can be shown. The images show that a gradual increment of temperature provokes a process of coarsening of pores, which gives membrane more consolidated at 1,273 K with both size particles. A narrow distribution can be seen at low firing temperature (1,073 and 1,173 K) (Fig. 10). However, over 1,373 K, the microstructure of the membrane shows an increasement in grain size; the particles melt together giving small cavities. We reported that a higher temperature produce a collapse in the porous structure creating more dense ceramic body. As a result the decreased porosity of the membrane by increasing the sintering temperature, we obtained lower permeance.

Through characterization, it was found that the pore size distribution of the membranes gradually increase with the increase of the particle size distribution (Figs. 10A–C vs. D–F).

A design experiment have been established in order to optimize the parameters of ceramic membranes synthesized (Figs. 11 and 12 and Table 6).

4. Conclusion

Highly ordered flat sheet membranes were successfully synthesized by mixing iron ore, methocel and amigel as well as starch with water which is the most commonly used solvent for cost and safety reasons. The characterization of the synthesized membranes have been controlled by mercury intrusion porosimetry, porometry method, permeance of air and water and finally we have been used the scanning electron microscopy to control the microstructure of the inner surface of the membranes.

On the basis of the whole work, the resulting pore size distribution for iron big and small size as obtained by mercury porosimetry and porometry method has been confirmed by scanning electron microscopy. After optimizing,

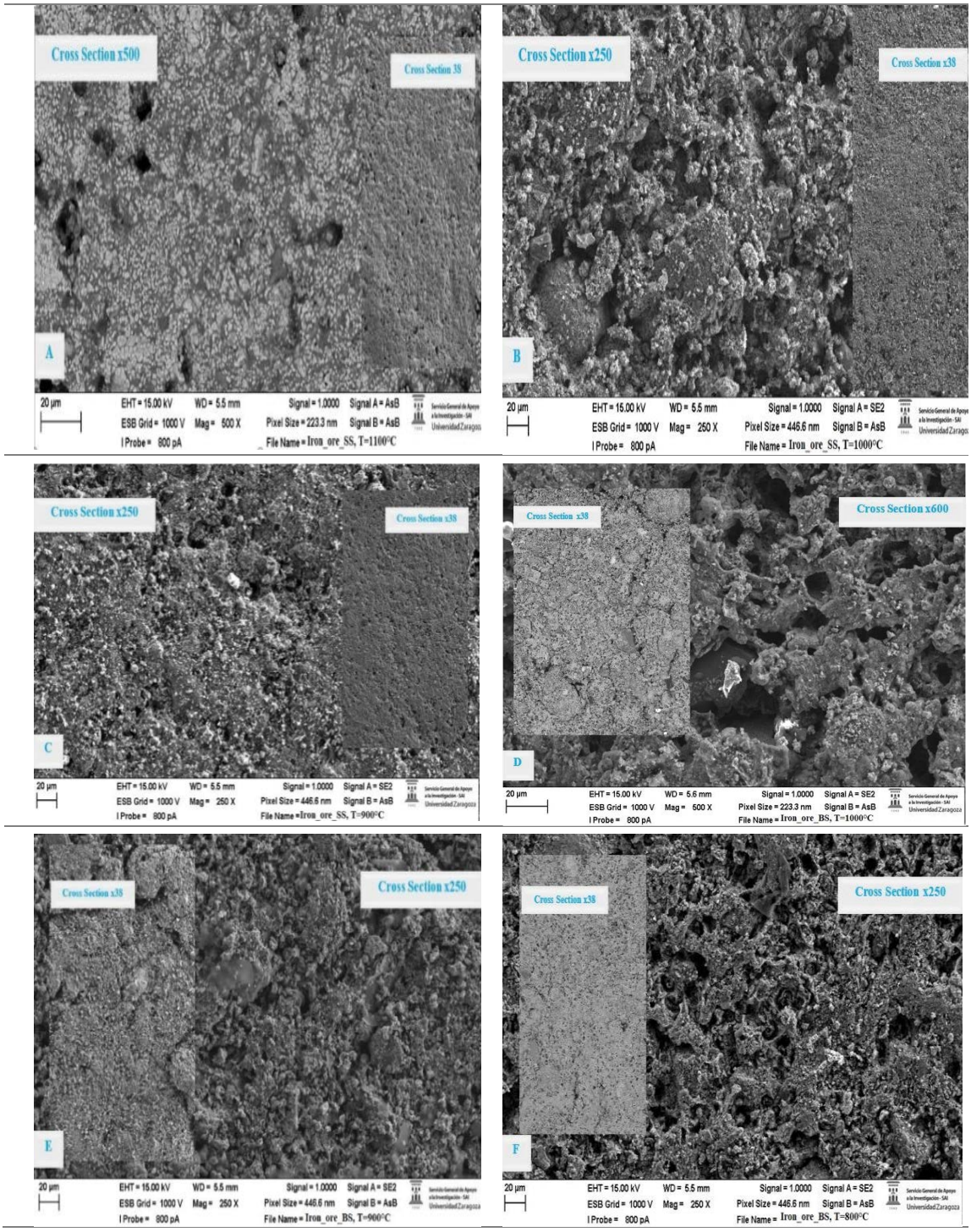

Fig. 10. Scanning electron microscopy photomicrograph of the different samples used. (A) Membrane fired at 1,373 K with Iron_ore_SS. (B) Membrane fired at 1,273 K with Iron_ore_SS. (C) Membrane fired at 1,173 K with Iron_ore_SS. (D) Membrane fired at 1,273 K with Iron_ore_BS. (E) Membrane fired at 1,273 K with Iron_ore_BS. (F) Membrane fired at 1,073 K with Iron_ore_BS.

ceramic membranes synthesized with $Iron_{SS}$ and $Iron_{BS}$ labeled A and E, respectively were found to process the optimal property in this study. The diameter of pores using mercury porosimetry were achieved 6.1 and 4.8 μm for sample A and E, respectively.

These investigations present a correlation with the results achieved with the permeance of air and water. Higher values of air permeance were obtained with $Iron_{BS}$. The highest water permeance was obtained at 1,273 K, which was 210^6 L/h/m^2·bar. For water permeance the membrane

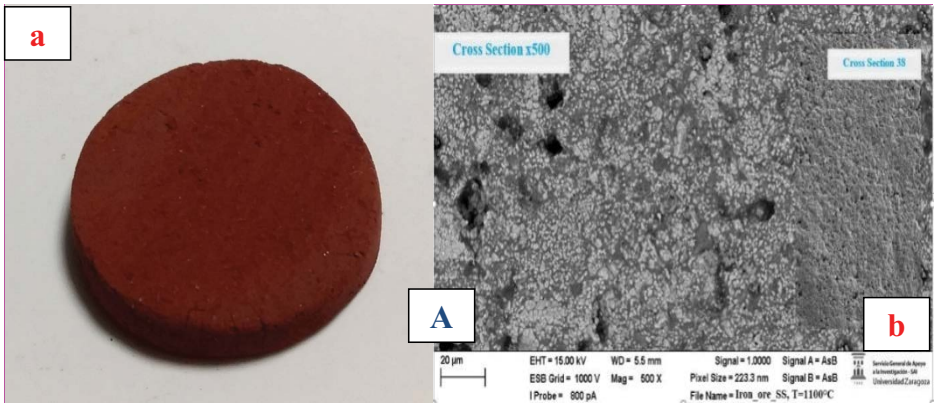

Fig. 11. Photograph (a) and scanning electron microscopy photomicrograph (b) of iron ore membrane (A) fired at 1,373 K for particles size smaller than 60 µm.

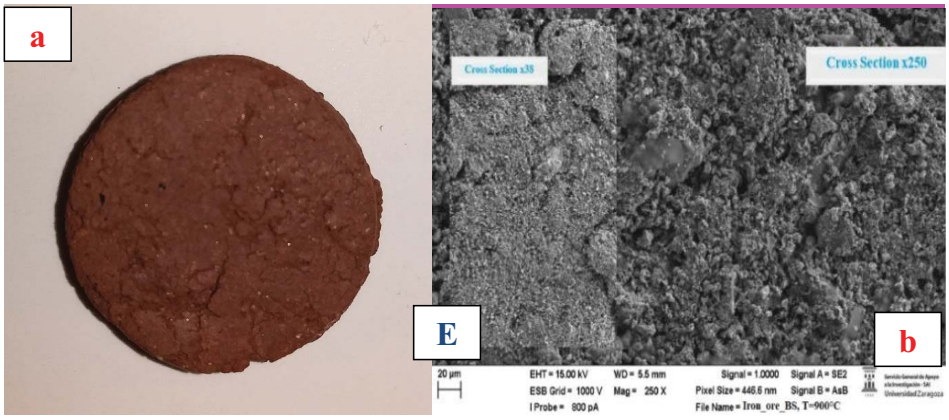

Fig. 12. Photograph (a) and scanning electron microscopy photomicrograph (b) of iron ore membrane (E) fired at 1,173 K for particles size in the range of (60–250 µm).

Table 6
Optimal parameters of ceramic membrane synthesized A and E

Parameters / Membrane types	Diameter	Thickness	Diameter of pores using mercury porosimetry	Air permeance	Water permeance
Membrane(E)	1.3 cm	0.3 cm	4.8 µm	856 × 10^3 L/h/m^2·bar	149 L/h/m^2·bar
Membrane(A)	1.3 cm	0.3 cm	6.1 µm	2 × 10^3 L/h/m^2·bar	281 L/h/m^2·bar

sintered at 1,273 K, with $Iron_{SS}$, was found to be the highest flat sheet membrane elaborated with 280.68 L/h/m^2·bar.

The challenge in the development of ceramic membranes based on iron ore provides great opportunities to produce an optimal inorganic membrane performance that is suitable for industrial applications and to explore the possibility of commercialization of our products.

Acknowledgement

The authors extended their appreciation to the Researchers Supporting Project number (RSP 2023R75), King Saudi University, Riyadh Saudi Arabia.

Declaration of competing interest

The authors declare that they have no known competing financial interests or personal relationships that could have appeared to influence the work reported in this paper.

Credit authorship contribution statement

All experiments were realized by R. Chihi and assisted by F. Ayari.

F. Ayari: writing, supervise, edition and submission.
R. Chihi: wrote the main manuscript text.

P. Ugarte and M. Menendez, participated in the realization of part 3.2 (Bubble point method and extended bubble point method) and at the interpretations of this experimental part.

L. Mansour participated in the characterization of initials materials (Figs. 1, 2, 6 and 10).

All authors reviewed the manuscript.

References

[1] S. Luque, D. Gómez, J.R. Álvarez, Industrial applications of porous ceramic membranes (pressure-driven processes), Membr. Sci. Technol., 13 (2008) 177–216.

[2] L. Palacio, Y. Bouzerdi, M. Ouammou, A. Albizane, J. Bennazha, A. Hernández, J.I. Calvo, Ceramic membranes from Moroccan natural clay and phosphate for industrial water treatment, Desalination, 245 (2009) 501–507.

[3] F. Bouzerara, A. Harabi, S. Achour, A. Larbot, Porous ceramic supports for membranes prepared from kaolin and doloma mixtures, J. Eur. Ceram. Soc., 26 (2006) 1663–1671.

[4] S. Masmoudi, R. Ben Amar, A. Larbot, H. El Feki, A. Ben Salah, L. Cot, Elaboration of inorganic microfiltration membranes with hydroxyapatite applied to the treatment of wastewater from sea product industry, J. Membr. Sci., 247 (2005) 1–9.

[5] A. Harabi, A. Guechi, S. Condom, Production of supports and filtration membranes from Algerian kaolin and limestone, Procedia Eng., 33 (2012) 220–224.

[6] A. Majouli, S. Alami Younssi, S. Tahiri, A. Albizane, H. Loukili, M. Belhaj, Characterization of flat membrane support elaborated from local Moroccan perlite, Desalination, 277 (2011) 61–66.

[7] A. Boulkrinat, F. Bouzerara, A. Harabi, K. Harrouche, S. Stelitano, F. Russo, F. Galiano, A. Figoli, Synthesis and characterization of ultrafiltration ceramic membranes used in the separation of macromolecular proteins, J. Eur. Ceram. Soc., 40 (2020) 5967–5973.

[8] A. Majouli, S. Alami Younssi, S. Tahiri, A. Albizane, H. Loukili, M. Belhaj, Characterization of flat membrane support elaborated from local Moroccan perlite, Desalination, 277 (2011) 61–66.

[9] F. Bouzerara, A. Harabi, B. Ghouil, N. Medjemem, B. Boudaira, S. Condom, Elaboration and properties of zirconia microfiltration membranes, Procedia Eng., 33 (2012) 278–284.

[10] A. Harabi, B. Boudaira, F. Bouzerara, L. Foughali, F. Zenikheri, A. Guechi, B. Ghouil, S. Condom, Porous Ceramic Supports for Membranes Prepared from Kaolin (DD3) and Calcite Mixtures, Proceedings of the 4th International Congress APMAS2014, April 24–27, Fethiye, Turkey, 2014, doi: 10.12693/APhysPolA.127.1164.

[11] B. Boudaira, A. Harabia, F. Bouzerara, S. Condom, Preparation and characterization of microfiltration membranes and their supports using kaolin (DD2) and $CaCO_3$, Desal. Water Treat., 9 (2009) 142–148.

[12] A. Bouazizi, M. Breida, A. Karim, B. Achiou, M. Ouammou, J.I. Calvo, A. Aaddane, K. Khiat, S. Alami Younssi, Development of a new TiO_2 ultrafiltration membrane on flat ceramic support made from natural bentonite and micronized phosphate and applied for dye removal, Ceram. Int., 43 (2017) 1479–1487.

[13] S. Saja, A. Bouazizi, B. Achiou, M. Ouammou, A. Albizane, J. Bennazha, S. Alami Younssi, Elaboration and characterization of low-cost ceramic membrane made from natural Moroccan perlite for treatment of industrial wastewater, J. Environ. Chem. Eng., 6 (2018) 451–458.

[14] J. Fang, G. Qin, W. Wei, X. Zhao, Preparation and characterization of tubular supported ceramic microfiltration membranes from fly ash, Sep. Purif. Technol., 80 (2011) 585–591.

[15] R. Chihi, I. Blidi, M. Trabelsi-Ayadi, F. Ayari, Elaboration and characterization of a low-cost porous ceramic support from natural Tunisian bentonite clay, C.R. Chim., 22 (2019) 188–197.

[16] A.A. Tireli, I. do Rosário Guimarães, J.C. de Souza Terra, R.R. da Silva, M.C. Guerreiro, Fenton-like processes and adsorption using iron oxide-pillared clay with magnetic properties for organic compound mitigation, Environ. Sci. Pollut. Res. Int., 22 (2015) 870–881.

[17] U. Schwertmann, R.M. Cornell, Iron Oxides in the Laboratory, Preparation and Characterization, Wiley-VCH, New York, USA, 2008, p. 188.

[18] L.C.A. Oliveira, T.C. Ramalho, E.F. Souza, M. Gonçalves, D.Q.L. Oliveira, M.C. Pereira, J.D. Fabris, Catalytic properties of goethite prepared in the presence of Nb on oxidation reactions in water: computational and experimental studies, Appl. Catal., B, 83 (2008) 169–176.

[19] N. Sankararamakrishnan, A. Gupta, S.R. Vidyarthi, Enhanced arsenic removal at neutral pH using functionalized multiwalled carbon nanotubes, J. Environ. Chem. Eng., 2 (2014) 802–810.

[20] R.M. Cornell, U. Schwertmann, The Iron Oxides: Structure, Properties, Reactions, Occurrences and Uses, VCH, Weinheim, Germany, 2003, pp. 158–164.

[21] N. Frini, M. Crespin, M. Trabelsi, D. Messad, H. Van Damme, F. Bergaya, Preliminary results on the properties of pillared clays by mixed Al-Cu solutions, Appl. Clay Sci., 12 (1997) 281–292.

[22] A.P. Grosvenor, B.A. Kobe, M.C. Biesinger, N.S. McIntyre, Investigation of multiplet splitting of Fe 2p XPS spectra and bonding in iron compounds, Surf. Interface Anal., 36 (2004) 1564–1574.

[23] D. Bikiaris, S. Daniilia, S. Sotiropoulou, O. Katsimbiri, E. Pavlidou, A.P. Moutsatsou, Y. Chryssoulakis, Ochre-differentiation through micro-Raman and micro-FTIR spectroscopies: application on wall paintings at Meteora and Mount Athos, Greece, Spectrochim. Acta, Part A, 56 (2000) 3–18.

[24] K.S.W. Sing, D.H. Everett, R.A.W. Haul, L. Moscou, R.A. Pierotti, J. Rouquerol, T. Siemieniewska, Reporting physisorption data for gas/solid systems with special reference to the determination of surface area and porosity (Recommendations 1984), Pure Appl. Chem., 54 (1985) 603–619.

[25] Y.H. Chen, Thermal properties of nanocrystalline goethite, magnetite, and maghemite, J. Alloys Compd., 553 (2013) 194–198.

[26] R.Z.A. Rashid, H.M. Salleh, M.H. Ani, N.A. Yunus, T. Akiyama, H. Purwanto, Reduction of low grade iron ore pellet using palm kernel shell, Renewable Energy, 63 (2014) 617–623.

[27] K. Mondal, H. Lorethova, E. Hippo, T. Wiltowski, S.B. Lalvani, Reduction of iron oxide in carbon monoxide atmosphere—reaction controlled kinetics, Fuel Process. Technol., 86 (2004) 33–47.

[28] A.A. Liabastre, C. Orr, An evaluation of pore structure by mercury penetration, J. Colloid Interface Sci., 64 (1978) 1–18.

[29] S. Lowell, J.E. Shields, Powder Surface Area and Porosity, B. Scarlett, Ed., Powder Technology Series, Wiley, New York, 1984, pp. 119–197.

[30] E. Honold, E.L. Skau, Application of mercury-intrusion method for determination of pore-size distribution to membrane filters, Science, 120 (1954) 805–806.

[31] T. Gumi, M. Valiente, K.C. Khulbe, C. Palet, T. Matsuura, Characterization of activated composite membranes by solute transport, contact angle measurement, AFM and ESR, J. Membr. Sci., 212 (2003) 123–134.

[32] A. Marmur, Equilibrium contact angles: theory and measurement, Colloids Surf., A, 116 (1996) 55–61.

[33] M. Mulder, Basic Principles of Membrane Technology, 2nd ed, Kluwer Academic Publisher, Netherlands, 1996, pp. 168–167.

[34] P. Shao, R.Y.M. Huang, X. Feng, W. Anderson, Gas-liquid displacement method for estimating membrane pore-size distributions, AlChE J., 50 (2004) 557–565.

[35] M.A. Rahman, M.A. Mutalib, K. Li, M.H.D. Othman, Chapter 10 – Pore Size Measurements and Distribution for Ceramic Membranes, N. Hilal, A.F. Ismail, T. Matsuura, D. Oatley-Radcliffe, Eds., Membrane Characterization, Elsevier, 2017, pp. 183–189.

[36] S. Lagdali, Y. Miyah, M. El-Habacha, G. Mahmoudy, M. Benjelloun, S. Iaich, M. Zerbet, M. Chiban, F. Sinan, Performance assessment of a phengite clay-based flat membrane for microfiltration of real-wastewater from clothes washing: characterization, cost estimation, and regeneration, Case Stud. Chem. Environ. Eng., 8 (2023) 100388, doi: 10.1016/j.cscee.2023.100388.